



# Real Time, Onboard-only Landing Site Evaluation for Autonomous Drones

by

Joshua Springer

Thesis proposal submitted to the School of Computer Science  
at Reykjavík University in partial fulfillment  
of the requirements for the degree of  
**Doctor of Philosophy**

November 2021

Thesis Committee:

Marcel Kyas, Supervisor  
Professor, Reykjavík University, Iceland

Gylfi Þór Guðmundsson, Supervisor  
Adjunct Professor, Reykjavík University, Iceland

Joseph Foley, Advisor  
Professor, Reykjavík University, Iceland

External Person, Examiner  
Role, University, Country

Copyright  
Joshua Springer  
November 2021

# Real Time, Onboard-only Landing Site Evaluation for Autonomous Drones

Joshua Springer

November 2021

## Abstract

Landing is a last, unsolved problem in autonomous multi-rotor drone flight. Many other tasks such as takeoff, waypoint-to-waypoint flight, and miscellaneous mission tasks (e.g. collection of images and video) have been reliably automated. Yet, autonomous landing remains largely a manual task because of its inherently risky, sensitive nature. The critical result of this is that fully autonomous mission cycles are just out of reach with current technology, in many contexts. Prior work towards autonomous multi-rotor landing has been subject to at least one of several disadvantages - either it depends principally on GPS and is therefore subject to possibly fatal inaccuracy (especially in Iceland), it has relied on detection of special markers (known a priori) with a downward facing camera (such that it may easily lose sight of the markers during approach and descent), it uses differences in pixel speed to deduce terrain topology (but therefore depends on motion), or it has depended on sophisticated ground stations to carry out the computationally expensive processing required for terrain analysis. The proposed research targets the problem of autonomous landing with the goal of creating an algorithm to reliably land multi-rotor drones with the following constraints: 1. having no prior knowledge of a landing site or GPS position, 2. executing in real time with a critical deadline, and 3. using only the limited computational environment onboard a drone.

Thus far, we have created and tested several drone platforms with 3 different flight control software stacks (ArduPilot, PX4, and DJI), which have revealed many challenges of operating drones in Iceland: low GPS accuracy, unpredictable winds, and the commonality of rain. While a large, weatherproof drone system can withstand wind and rain, low GPS accuracy has proven to be a real obstacle. DJI drones and flight controllers have shown to vastly out-perform others in this regard, and thus provide a good base moving forward. Further, we have tested landing algorithms based on fiducial markers in simulation, but differing from previous work in that we use a gimbal-mounted camera to allow it to track the marker over time. This has involved the further development of existing fiducial systems (April Tag and WhyCode) to optimize for execution on embedded hardware, and to test the accuracy of their orientation estimation. Finally, we have created a proof of concept of such algorithms on a physical drone.

Moving forward, we plan to expand on the following research questions: **RQ1.** With what methods can a drone autonomously identify a safe, previously unknown landing site? **RQ2.** What data do such methods require? **RQ3.** How can such methods execute in real time, and in the power-limited environment of a drone? We hypothesize that **H1:** A U-net, or variants such as Residual U-net with pre-/post-processing steps for image rectification and communication with flight control software will be able to recognize landing sights from drone sensor data. **H2:** This data can be point clouds from LIDAR units or RGBD (image + depth) cameras, which are small enough to be embedded onto a drone. **H3:** An embedded TPU, GPU, or FPGA will be able to execute the method onboard a drone in real time. We plan to generate training/testing data sets of LIDAR/RGBD point clouds in AirSim, and collect further testing data sets from the real world using our existing drone platforms. This data will serve as the basis for training several neural network models based on the U-net architecture. Promising algorithms will be optimized using pruning and will be tested for execution speed and power consumption on physical hardware. Any sufficiently fast/accurate methods will be tested in real landing scenarios.

# Ég veit ekki hvernig á að tala íslensku

Joshua Springer

November 2021

## Útdráttur

Morbi luctus, wisi viverra faucibus pretium, nibh est placerat odio, nec commodo wisi enim eget quam. Quisque libero justo, consectetur a, feugiat vitae, porttitor eu, libero. Suspendisse sed mauris vitae elit sollicitudin malesuada. Maecenas ultricies eros sit amet ante. Ut venenatis velit. Maecenas sed mi eget dui varius euismod. Phasellus aliquet volutpat odio. Vestibulum ante ipsum primis in faucibus orci luctus et ultrices posuere cubilia Curae; Pellentesque sit amet pede ac sem eleifend consectetur. Nullam elementum, urna vel imperdiet sodales, elit ipsum pharetra ligula, ac pretium ante justo a nulla. Curabitur tristique arcu eu metus. Vestibulum lectus. Proin mauris. Proin eu nunc eu urna hendrerit faucibus. Aliquam auctor, pede consequat laoreet varius, eros tellus scelerisque quam, pellentesque hendrerit ipsum dolor sed augue. Nulla nec lacus.

Suspendisse vitae elit. Aliquam arcu neque, ornare in, ullamcorper quis, commodo eu, libero. Fusce sagittis erat at erat tristique mollis. Maecenas sapien libero, molestie et, lobortis in, sodales eget, dui. Morbi ultrices rutrum lorem. Nam elementum ullamcorper leo. Morbi dui. Aliquam sagittis. Nunc placerat. Pellentesque tristique sodales est. Maecenas imperdiet lacinia velit. Cras non urna. Morbi eros pede, suscipit ac, varius vel, egestas non, eros. Praesent malesuada, diam id pretium elementum, eros sem dictum tortor, vel consectetur odio sem sed wisi.

Sed feugiat. Cum sociis natoque penatibus et magnis dis parturient montes, nascetur ridiculus mus. Ut pellentesque augue sed urna. Vestibulum diam eros, fringilla et, consectetur eu, nonummy id, sapien. Nullam at lectus. In sagittis ultrices mauris. Curabitur malesuada erat sit amet massa. Fusce blandit. Aliquam erat volutpat. Aliquam euismod. Aenean vel lectus. Nunc imperdiet justo nec dolor.

Etiam euismod. Fusce facilisis lacinia dui. Suspendisse potenti. In mi erat, cursus id, nonummy sed, ullamcorper eget, sapien. Praesent pretium, magna in eleifend egestas, pede pede pretium lorem, quis consectetur tortor sapien facilisis magna. Mauris quis magna varius nulla scelerisque imperdiet. Aliquam non quam. Aliquam porttitor quam a lacus. Praesent vel arcu ut tortor cursus volutpat. In vitae pede quis diam bibendum placerat. Fusce elementum convallis neque. Sed dolor orci, scelerisque ac, dapibus nec, ultricies ut, mi. Duis nec dui quis leo sagittis commodo.

## **Acknowledgements**

I would like to thank the Flying Spaghettii Monster and his noodly appendage.

# Contents

<b>1</b>	<b>Introduction</b>	<b>1</b>
1.1	Problem Statement and Motivation . . . . .	1
1.2	Background . . . . .	1
1.2.1	Autopilot Software/Hardware . . . . .	1
1.2.2	Simulation Software . . . . .	2
1.2.3	Robotics Software . . . . .	2
1.2.4	Fiducial Markers . . . . .	2
1.3	Related Work . . . . .	2
<b>2</b>	<b>Current Progress</b>	<b>3</b>
2.1	Building and Flying Two Hexacopters . . . . .	3
2.1.1	Results . . . . .	6
2.2	WhyCode Modifications . . . . .	7
2.2.1	Background . . . . .	7
2.2.2	Orientation Ambiguity . . . . .	8
2.2.3	Proposed Solutions . . . . .	10
2.2.4	Conclusion . . . . .	13
2.3	April Tag Modifications . . . . .	13
2.3.1	Re-testing in Simulation with April Tag 48h12 . . . . .	14
2.3.2	Testing on Physical Hardware, and the creation of April Tag 24h10 . . . . .	15
2.3.3	Testing with PX4's Precision Land . . . . .	15
2.3.4	Conclusion . . . . .	19
2.4	Experiments with AirSim . . . . .	19
2.5	Small Drone . . . . .	19
2.6	Heavy Lift Drone with Infrared Camera . . . . .	20
<b>3</b>	<b>Research Plan</b>	<b>22</b>
3.1	Data Set Generation . . . . .	22
3.2	Terrain Classifier Creation . . . . .	22
3.3	Testing in Simulation . . . . .	22
3.4	Testing on Physical Hardware . . . . .	22
3.5	Choice of Flight Software . . . . .	22
3.6	Risk Analysis . . . . .	23

# Chapter 1

## Introduction

### 1.1 Problem Statement and Motivation

The goal of the proposed research is to explore the topic of autonomous, unstructured drone landing. Current autonomous landing methods have at least one of the following disadvantages: they are blind to obstacles, they require previously *known* landing sites, they depend on sophisticated ground control stations for offloading of expensive computation. This proposed research targets a gap in current autonomous landing methods. Specifically, we aim to develop a method for quickly analyzing terrain and identifying safe landing sites using only embedded computational hardware and a minimal set of sensors.

Landing is a particularly difficult aspect of drone flight, owing mainly to its risky nature and required precision. As a result, most drone landings are carried out by (or under the supervision of) a human operator, inherently limiting the applicability of autonomous drones. Some autopilot software includes an Application Programming Interface (API) for *precision landing*, which allows a drone to localize and direct itself with respect to a landing pad during an autonomous landing, according to data provided by external sensors and programs. However, there is no particular method of autonomous landing in widespread use. As autonomous and semi-autonomous drones are not able to reliably handle landings on rough terrain or in non-ideal conditions, human operators often disable autonomous control during landing (opting for full manual control), or abuse/hack the landing system by descending to a low altitude, grabbing hold of the drone, and disabling the motors, as shown in Figure 1.1. Aside from potentially exposing users to dangerous rotors, this landing technique showcases the limitations induced by a lack of autonomous landing method.

In sufficiently flat, large areas, fully autonomous drone missions can end with a GPS-based autonomous landing which is blind to obstacles in the environment. However, intuitively and demonstrably, this can lead to crash-landings at landing sites that have obstacles within the error radius of the GPS, which can be anywhere from a few centimeters to a few meters. In the available open source autopilot softwares, obstacles are simply not handled, and drones will continue their landing attempts even if fatally obstructed.

### 1.2 Background

#### 1.2.1 Autopilot Software/Hardware

The most prominent, open source drone autopilot software packages are ArduPilot [1] and PX4 [7], which can integrate easily with many additional/custom software packages. DJI drones, while the most commonly used consumer-grade drones, use proprietary, closed source autopilot software that has a limited API for interacting with external software. Thus, ArduPilot and PX4 and custom drones are typically used for research on drones themselves, while DJI software



Figure 1.1: Non-ideal, human-assisted landing in the absence of an autonomous, safe landing method that considers the surrounding environment.

and drones are typically used for consumer/commercial tasks. ArduPilot and PX4 communicate using the same open source, customizable protocol - MAVLink [4] - which has APIs in many different programming languages as well as with Robot Operating System (ROS).

### 1.2.2 Simulation Software

### 1.2.3 Robotics Software

### 1.2.4 Fiducial Markers

## 1.3 Related Work

# Chapter 2

## Current Progress

### 2.1 Building and Flying Two Hexacopters

After finishing a master thesis [12] wherein I developed an algorithm for autonomously landing a drone using fiducial markers in simulation, the next step was to test this method on physical platforms. The algorithm required identifying fiducial markers through image analysis, tracking the markers via a gimbal-mounted camera, calculating position targets in order to direct the drone towards the landing pad, and communicating those position targets to the flight control software. The base frame for the drones are the Tarot 680 hexacopter kit, which provides a good thrust-to-weight ratio, good flight stability, and space for mounting multiple computational components. A combination of Raspberry Pi and Navio2 [5] shield serve as a flight controller which can communicate with a companion board. The companion boards (a Google Coral Dev board and an NVIDIA Jetson Nano) communicate via a USB network to the flight controller and perform all heavy computations involving image analysis, coordinate system transforms, PID control, and position target generation.

An overview the components is as follows:

- **11.1 V LiPo Battery:** this battery provides power to a battery eliminator circuit (BEC) for isolation of the power system for the computational electronics (the flight controller and companion board).
- **BEC (Battery Eliminator Circuit):** the BEC transforms 11.1V power to 5V power for the flight controller and companion board. The flight controller and companion board each have their own 4A channel to meet their given power requirements.
- **Flight Controller:** this combination of a Raspberry Pi 3 B+ and Navio2 shield runs the ArduPilot software to control the drone, and communicates with the companion board to control the gimbal.
- **Telemetry Radio:** the telemetry radio provides two-way communication between the flight controller and a ground control station that is also fitted with its own telemetry radio. It is connected to the flight controller via USB. The software on the ground control station provides an interface for real-time status messages and sending high-level commands.
- **RC Receiver:** the RC receiver provides a one-way radio link between the pilot's transmitter and the flight controller, allowing the pilot to manually control the drone. It is connected to the flight controller via SBUS which provides an 8-channel multiplexed PWM signal to reduce the needed wires and space. This provides an interface for control by a human pilot, which is often used in testing but will eventually be mostly unused.
- **22.2 V LiPo Battery:** this battery provides power to the speed controllers and gimbal.



Figure 2.1: Hardware Setup

- **Speed Controllers:** the speed controllers receive a PWM signal from the flight controller which indicates a throttle value. They then provide corresponding power signals to the motors.
- **Motors:** the motors spin propellers to provide thrust in order to control the drone's position in the air.
- **Gimbal:** the gimbal controls the orientation of the camera based on PWM signals from the flight controller which indicate target angles. Its onboard IMU and driver filter the motion of the camera in order to provide a smooth camera image.
- **Companion Board:** the companion board reads an image from the camera and calculates the position of the landing pad relative to the drone. It then communicates this information to the flight controller via an Ethernet over USB connection using ROS.

The computational components require some protection from the harsh Icelandic weather, and we therefore designed and 3D-printed a component mounting plate with a connector for a canopy. We also designed and printed cases to protect camera modules and allow them to be mounted in a gimbal with a GoPro form factor. The final versions of these components (after several iterations) can be seen in Figure 2.2. The fully assembled hexacopters are shown in Figure 2.3

The algorithm is implemented as a set of ROS modules, as explained below:

1. `gscam` retrieves camera input and makes it available as a ROS topic,
2. `whycon_ros` analyzes camera images to detect WhyCon/WhyCode markers and determine their pose,
3. `gimbal_controller` reads the poses of any detected markers, passes this information as input to two PID systems, converts the output of the PID systems to PWM outputs, and forwards the PWM outputs to the autopilot software to control the gimbal.
4. `landing_controller` reads the poses of any detected markers, performs coordinate system transforms to generate a target position, and forwards them to the autopilot software.



Figure 2.2: 3D printed parts for the Tarot hexacopters.



Figure 2.3: The assembled drones and their electronics compartments.

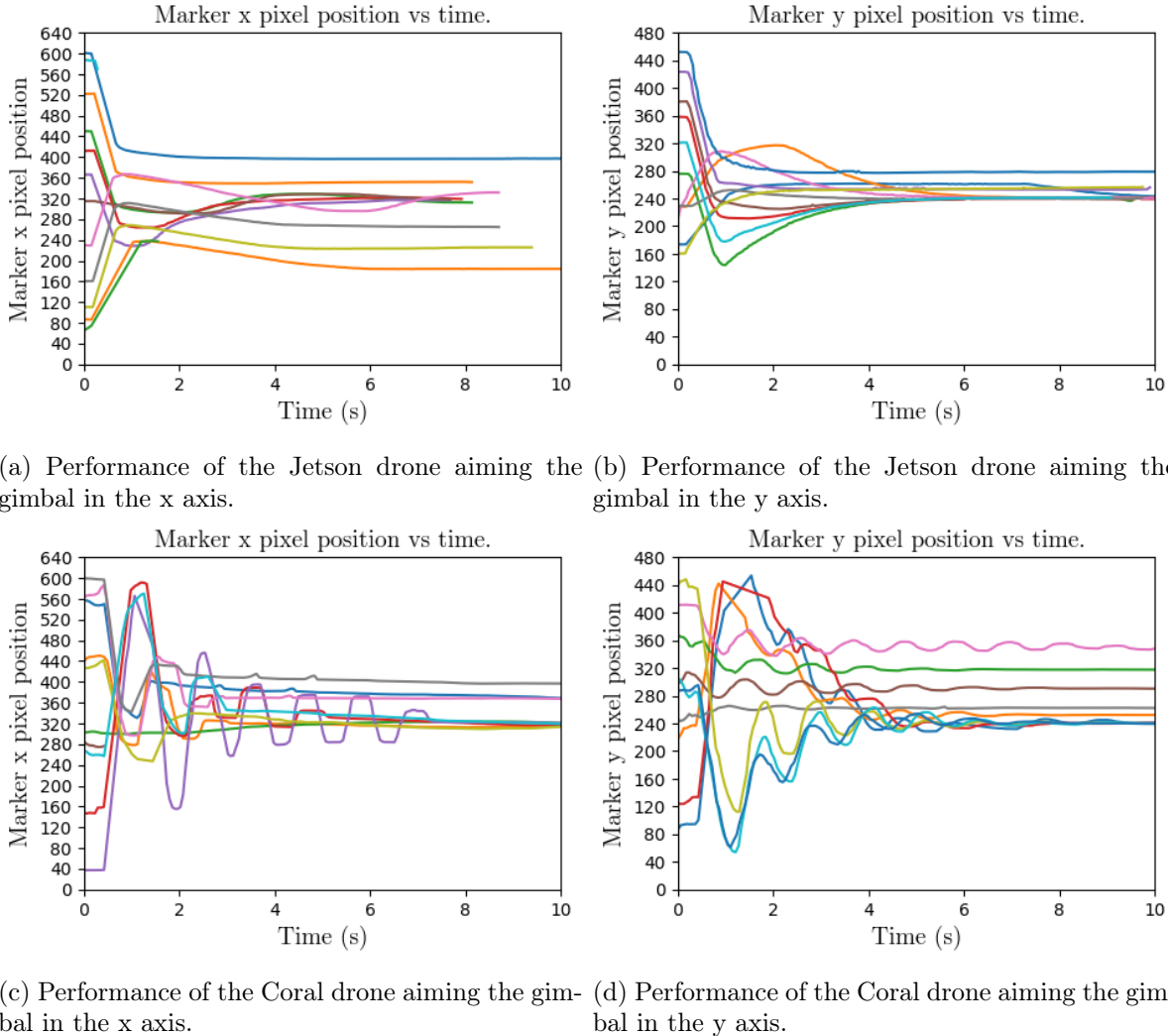


Figure 2.4: Performance of aiming the gimbals.

### 2.1.1 Results

The drones fly with good stability even in high winds, with an estimated 15-20 minute flight time.

<sup>1</sup> In lab tests and in flight, they are able to detect and track fiducial markers using the method tested in simulation. However, only the more lightweight WhyCon/WhyCode fiducial system was used in testing, instead of the April Tag system, because of the time constraints of this summer project. The performance of the drones in tracking the markers is shown in Figure 2.4, where each subfigure shows the position of the marker in the camera frame in the given axis, with a resolution of 640x480 pixels after resizing in order to decrease the computational requirements of the image analysis. The wide angle lens of the Jetson Nano camera module results in much smoother tracking, since each pixel corresponds to a larger distance than with the Google Coral camera module.

The drones are able to approach the landing pad autonomously, but have not yet touched down autonomously. This is due to two principal factors. First, GPS precision is low in Iceland (i.e. geometric dilution of precision (GDOP) is relatively high) because of Iceland's distance from the equator. Methods of autonomous positioning within the ArduPilot framework which were not ostensibly GPS-based are eventually translated into lat/lon/alt position targets, and the drones attempted to navigate to them with GPS only (instead of other methods such as dead

---

<sup>1</sup>Video of some of the flights and landing attempts can be found at: <https://vimeo.com/461576798>

reckoning). Since the GDOP was prohibitively high, the drones could not accurately estimate their position. Therefore, they could only follow a coherent path for a limited amount of time when navigating autonomously, after which the trajectory was unpredictable, even if the position target commands were correct.

Second, there is a fundamental challenge with fiducial markers which comes as a result of the limitations of embedding 2-dimensional shapes into 3-dimensional spaces. While the position of the marker in the camera frame can be detected unambiguously, the orientation of the marker cannot. Especially when the marker is almost normal to the camera's view, its orientation becomes increasingly ambiguous in the roll and pitch components. (This can be intuitively visualized by imagining the difference between the appearances of a marker when it is at  $(R, P, Y) = (1^\circ, 0, 0)$  versus when it is at  $(R, P, Y) = (-1^\circ, 0, 0)$ . These orientations would be difficult to distinguish even for the human eye, and much more difficult for a camera with 640x480 pixels.) Tests in simulation revealed this phenomenon, however, because of a variety of factors (a more “perfect” camera/marker/world, better GPS, lack of logistical constraints, etc.), this phenomenon was not prohibitive in simulation, and successful landings were plentiful.

These two problems set the stage for more research and modifications to the fiducial systems, outlined in Sections 2.2 and 2.3.

## 2.2 WhyCode Modifications

### 2.2.1 Background

The WhyCon fiducial marker, shown in Figure 2.5 consists of a white circle inside of a larger black circle. The identification algorithm is computationally simple:

- An input image is searched for white regions.
- The detector flood-fills and determines a measure of circularity for each white region.
- The detector seeks a black region directly outside of each white region, flood fills it, and determines a measure of circularity for it.
- The circularity measures are compared, and the white/black region combination is called a WhyCon marker if it is adequately circular (under projection).
- The position of the marker is determined using the pinhole model of a monocular camera with known intrinsic parameters (pixel resolution, lens distortion, principal points, focal lengths), and the diameter of the marker.
- The major and minor axes of the elliptical regions provide a basis from which to determine the marker’s orientation.

The WhyCon software’s purpose is to determine the pose (position *and* orientation) of detected WhyCon markers with respect to the camera field of view. The position of the markers can be determined with centimeter accuracy in most use cases. However, the full radial symmetry of the WhyCon marker inherently prevents the assignment or recognition of a “yaw” orientation - that is, only two components of the marker’s rotation can be determined.

WhyCode expands on WhyCon to add an ID and yaw orientation to the plain WhyCon marker. While the majority of the detection algorithm is the same, an ID is encoded onto the marker in the form of a Manchester encoding that is wrapped around the inner, white circle, as shown in Figure 2.6. By sampling along the circle halfway between the white circle and black circle, the detector can determine the ID encoding. Figure 2.7 shows potential collisions between WhyCode markers that are rotationally symmetric but have different IDs. While it is impossible to distinguish between rotationally symmetric markers, this problem can be overcome



Figure 2.5: WhyCon marker.

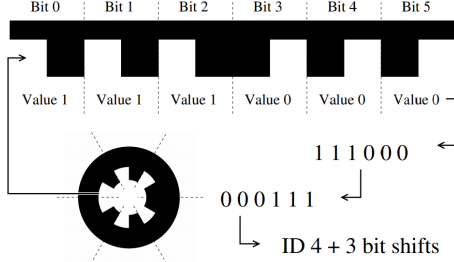


Figure 2.6: WhyCode ID Manchester “Necklace” Encoding.

by bit-shifting the ID’s binary string to its lowest value in all cases before determining the ID. This also gives a means of determining a “yaw origin” so that the orientation of the marker can be determined in 3 dimensions.

### 2.2.2 Orientation Ambiguity

In contrast to the accurately/unambiguously recognizable position of WhyCode markers, the orientation is ambiguous in many circumstances, as can be seen in Figure 2.8, particularly during time  $t \in [4, 8]$ . This ambiguity comes from the fact that the orientation is principally calculated from the semi-axes of the marker’s ellipses under the assumption that the marker is truly a circle. Calculating the orientation based on these semi-axes gives *two* candidate solutions that satisfy the assumption that the marker is facing the camera, and it is difficult to determine which of these candidates represents reality, especially when the marker is normal or near-normal to the camera’s field of view. The original WhyCode software [8] arbitrarily chooses the first solution as correct, and as such it does not need much analysis except to say that it has a high likelihood of choosing the wrong solution.

In the context of fiducial-based drone landing, the issue of orientation ambiguity affects a drone’s ability to estimate its own pose when its camera is mounted on a gimbal. Many gimbals do not output their orientations to the flight controller, and their orientations cannot be directly calculated from control signals in many cases, since many gimbals have sophisticated control systems. While a control signal may communicate a *target* orientation, many gimbals have their own IMU and take into account angular motion and acceleration in addition to a control signal. Therefore, it is difficult to determine the orientation of the gimbal simply based on its control

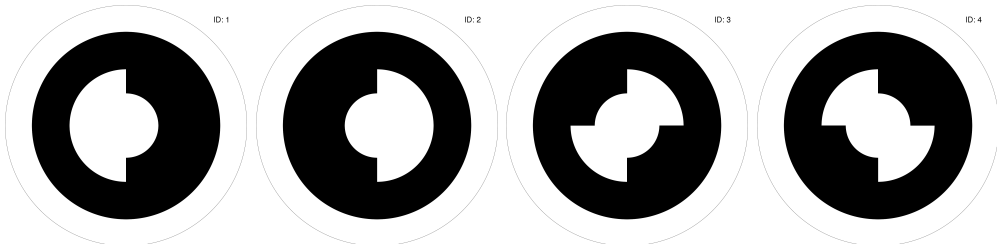


Figure 2.7: Rotational symmetry in 2-bit WhyCode markers.

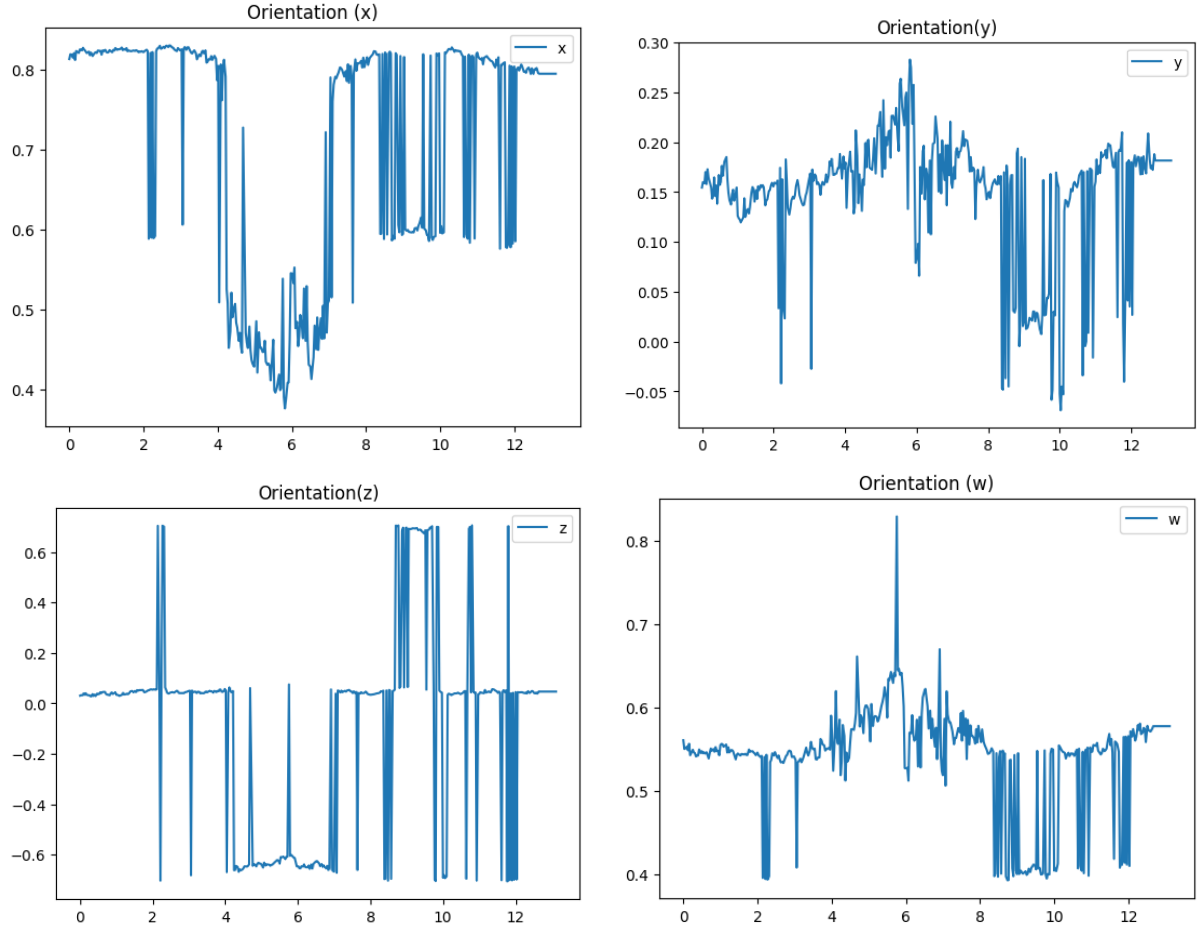


Figure 2.8: Components of the orientation quaternion for a WhyCode marker. Emphasis is placed on the discontinuities in all components, and sign flipping in the Z component.

signals. Without the orientation of either the fiducial marker *or* the gimbal, more assumptions about the landing scenario are required, such as (for example) that the camera is facing directly down always.

When a drone uses a fiducial marker to determine its position with respect to a landing pad without the assumption that its camera is in a fixed orientation, it can (theoretically) use the marker’s perceived orientation instead. The drone can rotate the marker’s *position* by the inverse of its *orientation* in order to determine its own position in the reference frame of the marker. However, such transformations, which depend on the ambiguous orientation of the marker, also exhibit such ambiguities - discontinuities in the orientation ultimately result in discontinuities in the perceived location of the drone.

Refinements of the WhyCon/WhyCode software, such as that proposed by Jiri Ulrich [13] (shown in ) attempt to disambiguate the orientation, with partial success. This method assumes that all “teeth” that form the marker’s ID should have the same number of sample points, and therefore chooses the candidate solution that has lower variance of the number of sample points per tooth. The samples are collected along the ellipse that is halfway between the white and black ellipses of the marker. The candidate solutions predict this ellipse to be in slightly different places, owing to the distortion caused by the camera lens. The rationale for the method is that the correct solution should predict the ellipse to be in its correct place, minimizing the variance in the number of sample points that coincide with each tooth. Conversely, the incorrect solution should predict the ellipse to be in the incorrect place, and therefore fewer sample points should coincide with teeth one side, increasing the variance. This provides a baseline on which

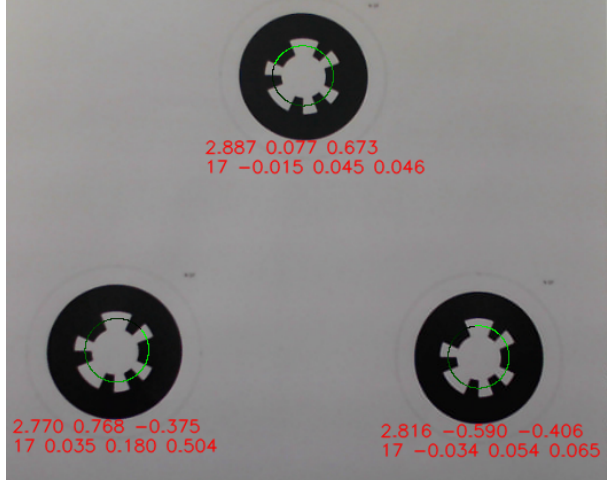


Figure 2.9: Example from Jiri Ulrich’s code, showing the circular sampling locations.

to disambiguate the solutions, but does not reliably choose the correct one, especially as the candidate solutions get closer and closer and the marker becomes more and more normal to the camera.

### 2.2.3 Proposed Solutions

As part of this project, I explore two different ways of solving the orientation ambiguity.

#### Radial Tooth Edge Sampling

The first method (the `ellipse_sampling` branch of [11]) is similar to that proposed by Jiri Ulrich, in that it is based on decreasing variance in sample points along the teeth. After the two candidate solutions for the orientation and the marker ID have been determined, a second phase of sampling begins. Each candidate solution predicts the center of the inner, white circle in pixel coordinates. (Since this system is designed to be lightweight, the center is not actually calculated, nor needed, to determine the position of the marker, and explicit calculation of this center is neglected by default.) Given the structure of WhyCode markers, we can assume that the circle along which the ID is sampled has a radius of  $1.5r$ , where  $r$  is the radius of the inner circle, and the radius of the circle bounding the teeth is  $2r$ . Further, from the ID sampling, we can identify the angle that goes through the center of each tooth. This makes it possible to test how well the candidate solution is centered on the marker at many points, and leverages the fact that camera distortion increases (and therefore prediction errors increase in magnitude) as one moves away from the center of the image.

The method does decrease the number of discontinuities in the perceived camera location, as shown in Figure 2.12, at the cost of significantly more sample points (more than double the original number). Unfortunately, it does not eliminate the discontinuities enough to justify the additional computational requirements.

#### Co-planar Markers

The second method works under the assumption that all markers are co-planar. Since the WhyCode system can accurately and quickly determine the positions of the markers, this assumption allows the orientation of co-planar markers to be determined unambiguously, *when 3 or more markers are detected simultaneously*. For each input image, the WhyCode algorithm identifies all markers and stores their positions. Additional code assumes that the markers are in a co-planar “bundle” and attempts to find the normal vector to the plane implied by the markers’ locations

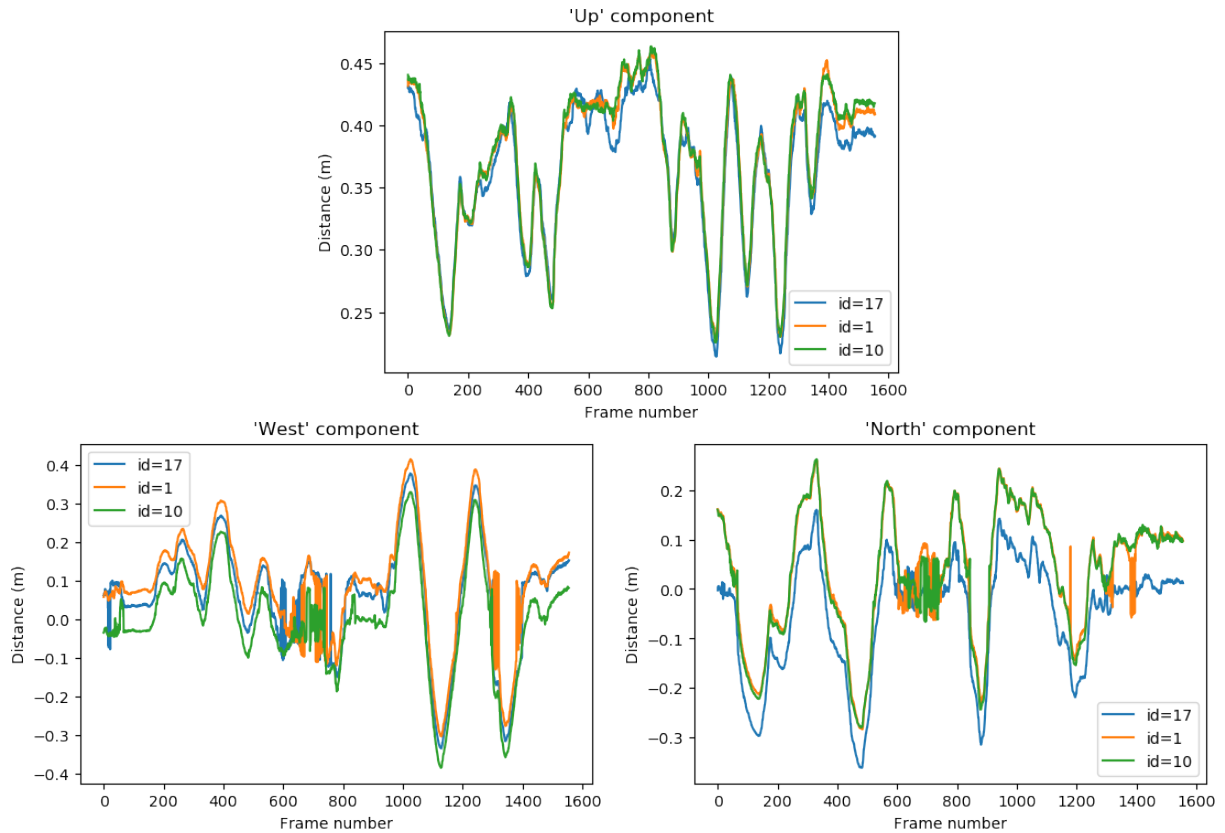


Figure 2.10: Each of the components of the perceived camera translation for 8-bit WhyCode markers with IDs 1, 10, and 17, using Jiri Ulrich's decision metric. The discontinuities occur mostly in the "west" and "north" components between frames 600 and 800, but also between frames 1200-1400.

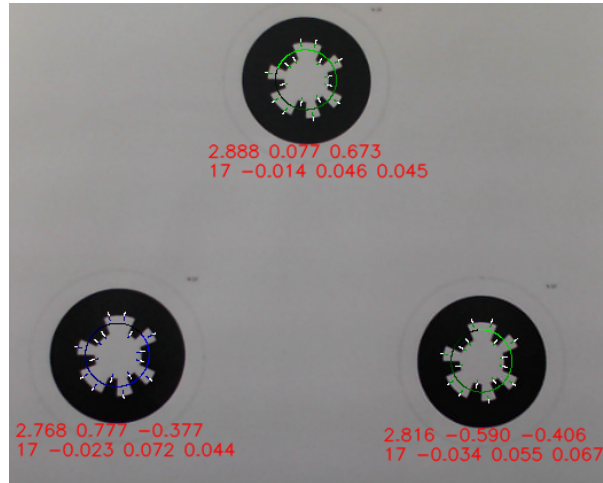


Figure 2.11: Example of sampling WhyCode markers on the radial edges of the teeth. The black/blue circle illustrates ID sampling locations, with the bluest samples occurring first, and blackest samples occurring last. Each of the blue/white radial line segments illustrates the sampling of the predicted edges of the teeth. The method chooses that solution that minimizes the variances of the ratio of blue to white on these line segments.

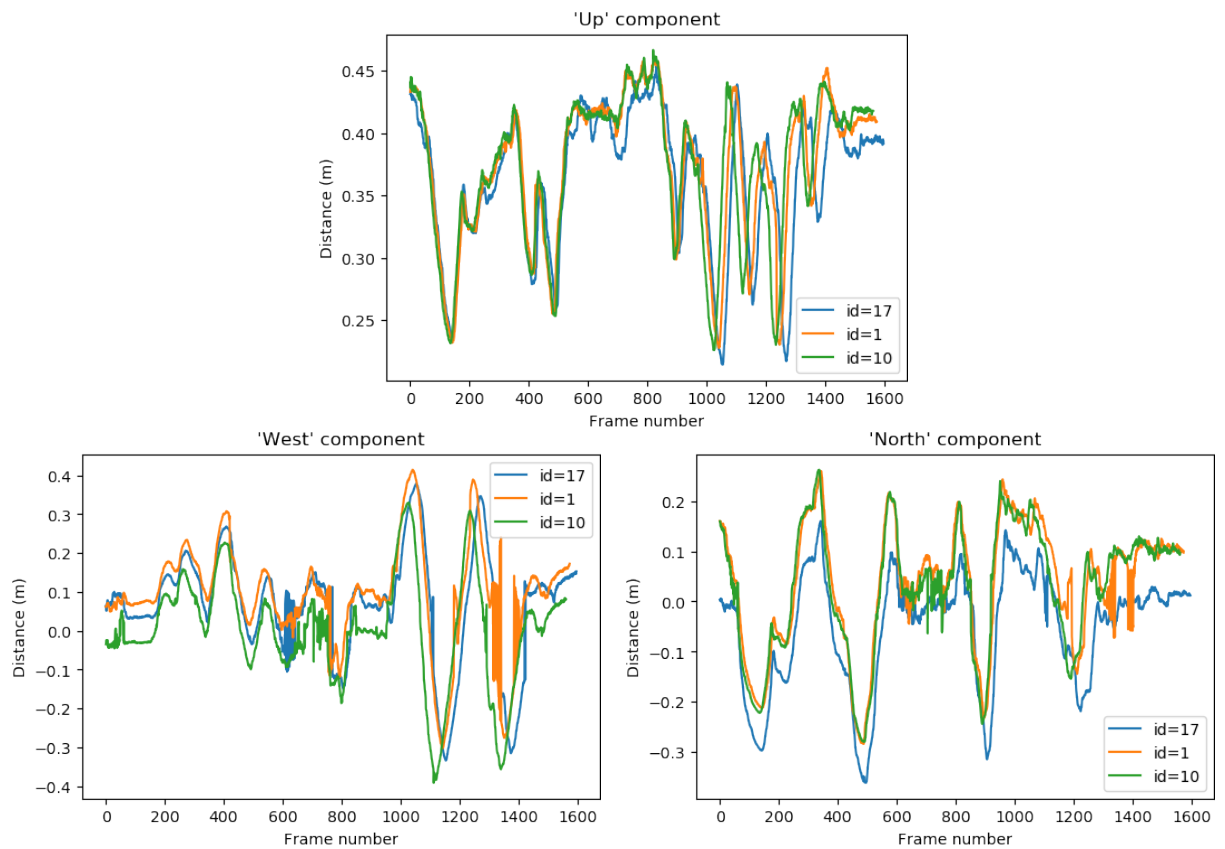


Figure 2.12: Each of the components of the perceived camera translation for 8-bit WhyCode markers with IDs 1, 10, and 17, using the tooth edge sampling decision metric. The discontinuities still occur mostly in the "west" and "north" components between frames 600 and 800, but also between frames 1200-1400.

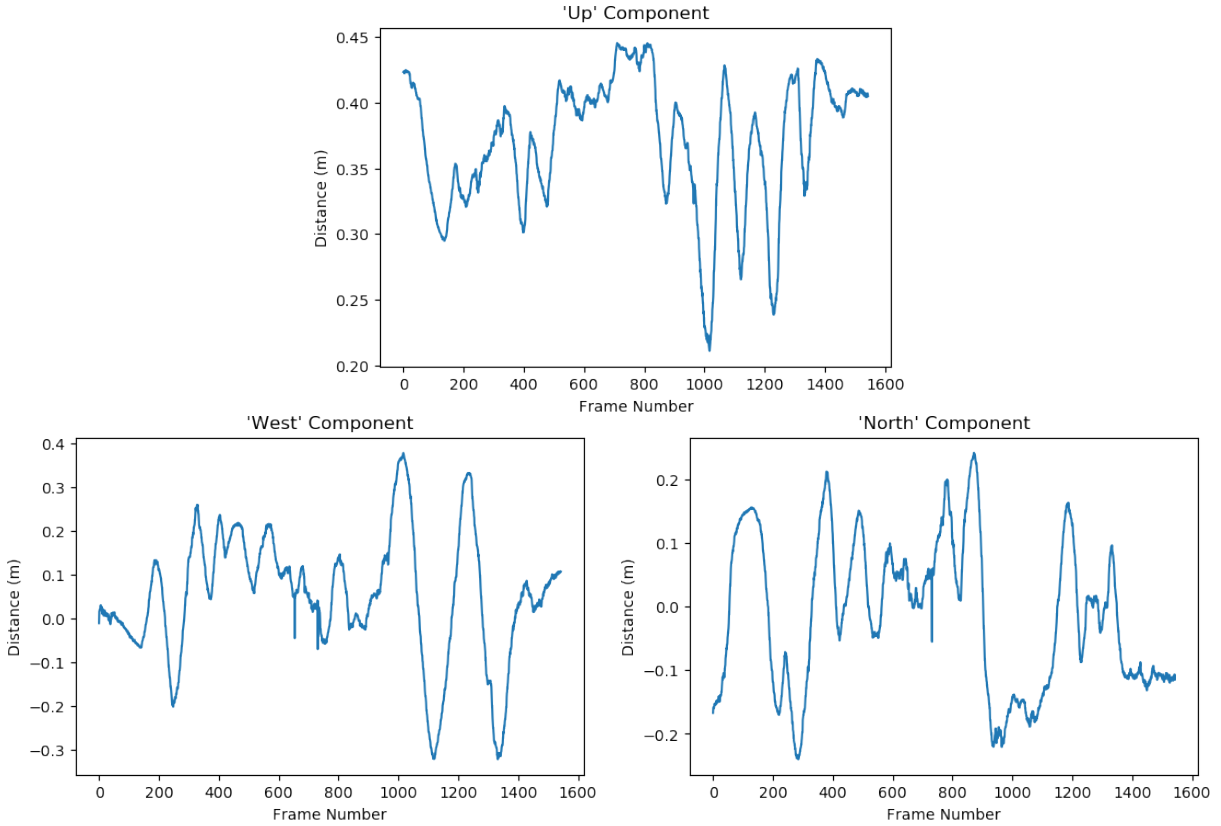


Figure 2.13: Each of the components of the perceived camera translation for a “bundle” of co-planar 8-bit WhyCode markers with IDs 1, 10, and 17. This algorithm significantly reduces the number of discontinuities.

using regression. The normal vector is used to calculate the pitch and roll components of the bundle’s orientation. The yaw of the bundle is assigned to be the yaw of the markers, which is determined unambiguously from the ID. The position of the bundle is the average position of its constituent markers.

This algorithm significantly reduces the number of discontinuities in the perception of the camera location, as shown in Figure 2.13. This comes at the computational cost of performing a regression to calculate the orientation of the plane at each frame. It also adds additional constraints: at least 3 co-planar (and non-collinear) markers must be visible at all times. This is problematic with a system such as WhyCode, which does not allow for embedding markers within other markers, because the required view area increases significantly to accommodate 3 markers simultaneously.

#### 2.2.4 Conclusion

WhyCode, though a powerful and computationally efficient fiducial system, is not well-suited to the task of landing a drone with a gimbal-mounted camera. While the system provides accurate, efficient, and scalable position estimation, the ambiguities and discontinuities in its orientation estimation prevent the required pose transformations without prohibitively expensive algorithmic extensions or constraints.

### 2.3 April Tag Modifications

April Tag [9][14][6] is a popular fiducial marker formed by a series of black and white squares. Several marker families are available, each with its own layout, as shown in Figure 2.14. The

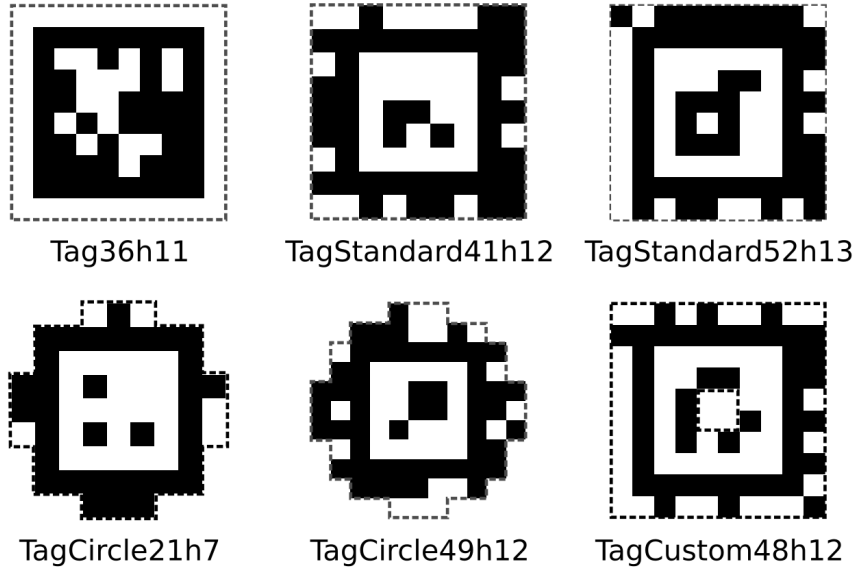


Figure 2.14: Several available April Tag families (from the paper Flexible Layouts for Fiducial Tags [6])

essential parts of the marker include a square border of black squares with a white border on the inside. Other square sections can either be “data bits” which contribute to the ID of the marker, or they can be unused and either not contribute to the marker definition at all, or provide a place for embedding another tag.

April Tag markers, in contrast to WhyCode markers, cannot be recognized independently of their ID. A benefit of this is that each marker can be assigned its own size before runtime, so many markers of different sizes and IDs can be used simultaneously. Figure 2.14f shows the family April Tag 48h12, which has 48 ID bits, and where each valid ID has a hamming distance of at least 12 from the others. When the April Tag family is generated, all arrangements of black and white squares that fit the requirements of the family definition (as well as isomorphic versions) are put into a hash table that is used to determine the validity of detected tags at runtime.

The 48h12 family has 4 undefined bits in its center, where another marker in the same family can be placed. This marker embedding is crucial for drone landing because it allows the drone to have reliable pose estimation throughout the entire landing. For example, if a landing pad uses a single marker that is recognizable from far away, it is likely that the marker will not be visible during the last stages of landing where the marker may eclipse the camera’s field of view. Non-embedded markers of different sizes can be placed on a landing pad in non-intersecting positions, but this implies more complications in tracking the markers during landing. Embedding concentric markers in one another and marking them as a tag bundle reduces the complexity regarding coordinate system transforms and tracking. The 48h12 family is therefore a natural candidate for marking landing pads.

### 2.3.1 Re-testing in Simulation with April Tag 48h12

After moving away from the WhyCode system for the purpose of autonomous landing, I re-implemented the method from the thesis to use only embedded 48h12 April Tags and re-tested successfully in simulation. The re-implementation involved adding to the April Tag ROS code with special focus on tag bundles, marker tracking, and coordinate system transforms. The landing pads are defined as concentric, co-planar tag bundles with the same yaw orientation that

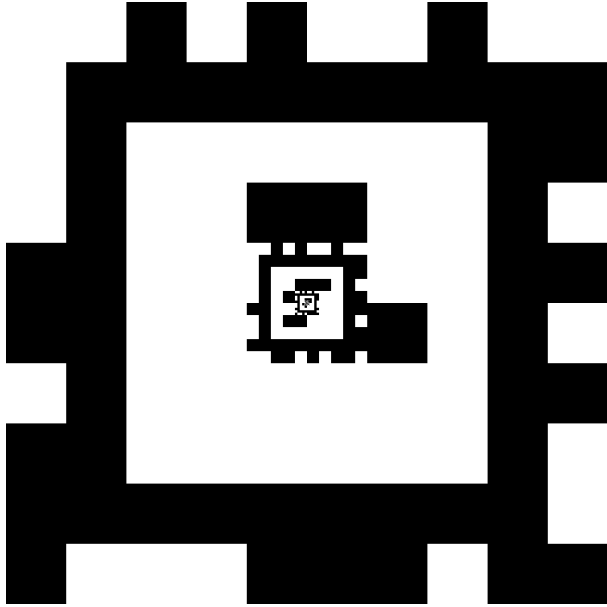


Figure 2.15: The landing pad for the given tests, with 48h12 IDs 3, 2, 1, and 0 in order of decreasing size.

take the position and orientation of their largest detected marker, expose their pixel centers  $u, v$  (for PID tracking), and calculate their camera translation (position rotated by the inverse of their orientation) before exposure to other ROS nodes through messages. The code is available at its Github repository [2]. The marker bundle forming the landing pad is shown in Figure 2.15.

The re-implementation was successful in simulation<sup>2</sup>, as shown by the landing trajectories in Figure 2.16. Additionally, the marker bundle tracking allowed for robust, uninterrupted tracking during landing, as shown by Figure 2.17.

### 2.3.2 Testing on Physical Hardware, and the creation of April Tag 24h10

A fundamental limitation of simulation in general is that it does not allow one to test all aspects of a given system. In contrast to simulated experiments on a desktop, which could easily run April Tag 48h12 at  $\geq 30$  Hz, initial experiments on a Raspberry Pi 3 showed that the system was only able to analyze 640x480 pixel images at a rate of 1.5Hz, which is not sufficient for a precision landing. Additionally, the 42211 markers of the 48h12 family create a huge ( $> 1$  GB) hash table on the Raspberry Pi, needlessly hogging valuable memory. However, no other default family of April Tags allows for marker embedding. This necessitated a new marker family that both allows for marker embedding and has sufficiently fast runtime performance on embedded hardware such as a Raspberry Pi 3 - April Tag 24h10. This family attempts to minimize the size of the markers, maximize the number of marker IDs in the family, and maintain the ability to embed markers. The definition is shown in Table 2.1, and the set of valid markers in Figure 2.18.

### 2.3.3 Testing with PX4’s Precision Land

April Tag is subject to orientation ambiguity, similar to the WhyCon/WhyCode markers mentioned in Section 2.2. When conducting an autonomous landing via a series of position setpoints, such as in the original thesis [12], the orientation ambiguity is not prohibitively destructive - essentially because the orientation is correct “most of the time.” However, when using a method

---

<sup>2</sup>Video from testing this method in simulation with April Tag 48h12 embedded markers can be found here: <https://vimeo.com/manage/videos/526223833>

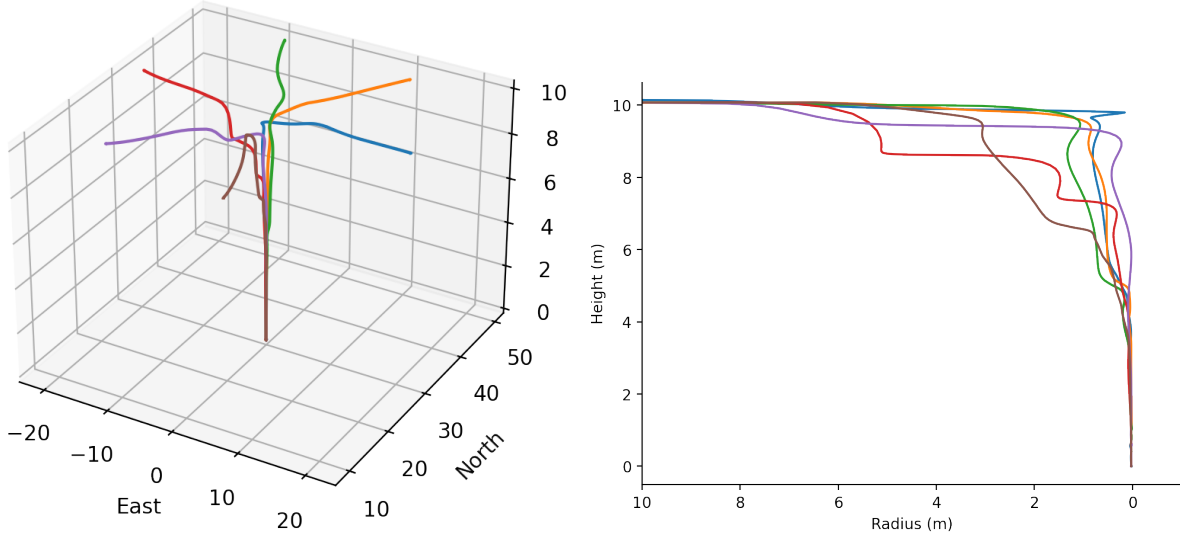


Figure 2.16: Left: landing trajectories for a series of simulated landings, centered around the landing pad. Right: the horizontal distance of the drone from the landing pad versus its height during landing. Both: these landings are executed by the code from the original thesis, using ArduPilot.

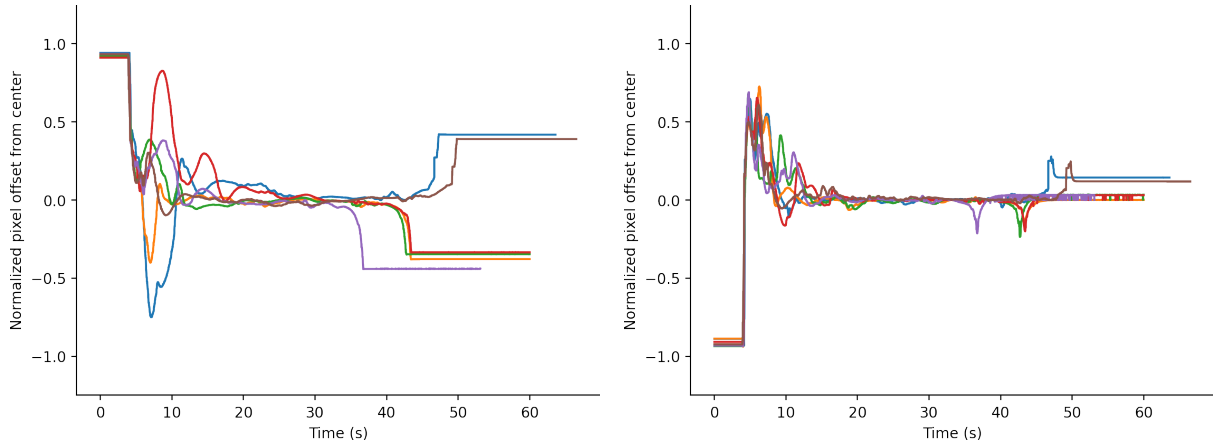


Figure 2.17: Pixel positions of the landing pad marker bundle during the landings depicted in Figure 2.16.

d	d	d	d	d	d	d
d	w	w	w	w	w	d
d	w	b	b	b	w	d
d	w	b	x	b	w	d
d	w	b	b	b	w	d
d	w	w	w	w	w	d
d	d	d	d	d	d	d

Table 2.1: Definition for the April Tag 24h10 family. Each square is marked by a letter representing its function. Data squares are marked as ‘d,’ white squares as ‘w,’ black squares as ‘b,’ and unused squares as ‘x.’

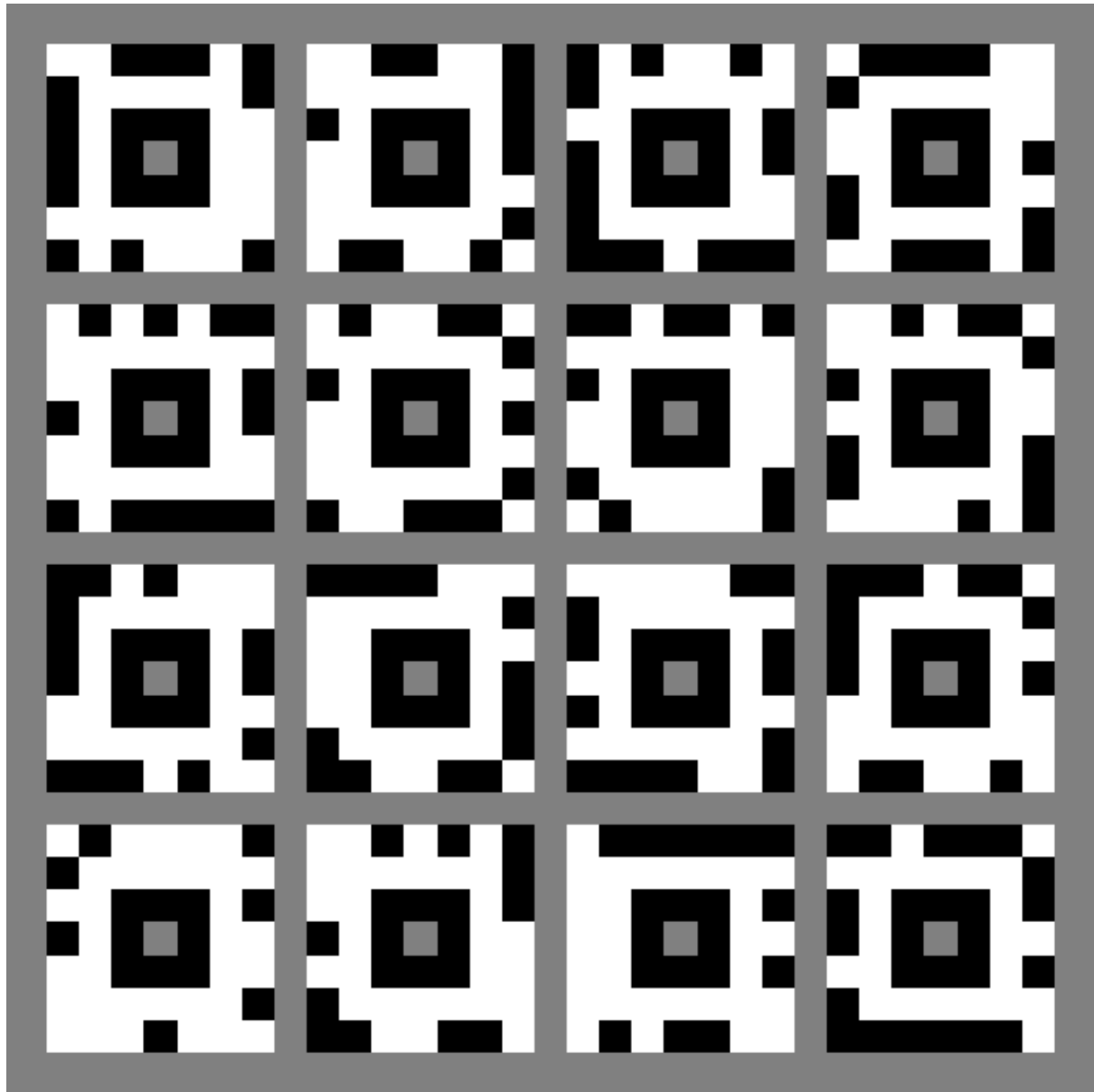


Figure 2.18: The set of markers in the April Tag 24h10 family. The grey squares are not part of the marker definitions.

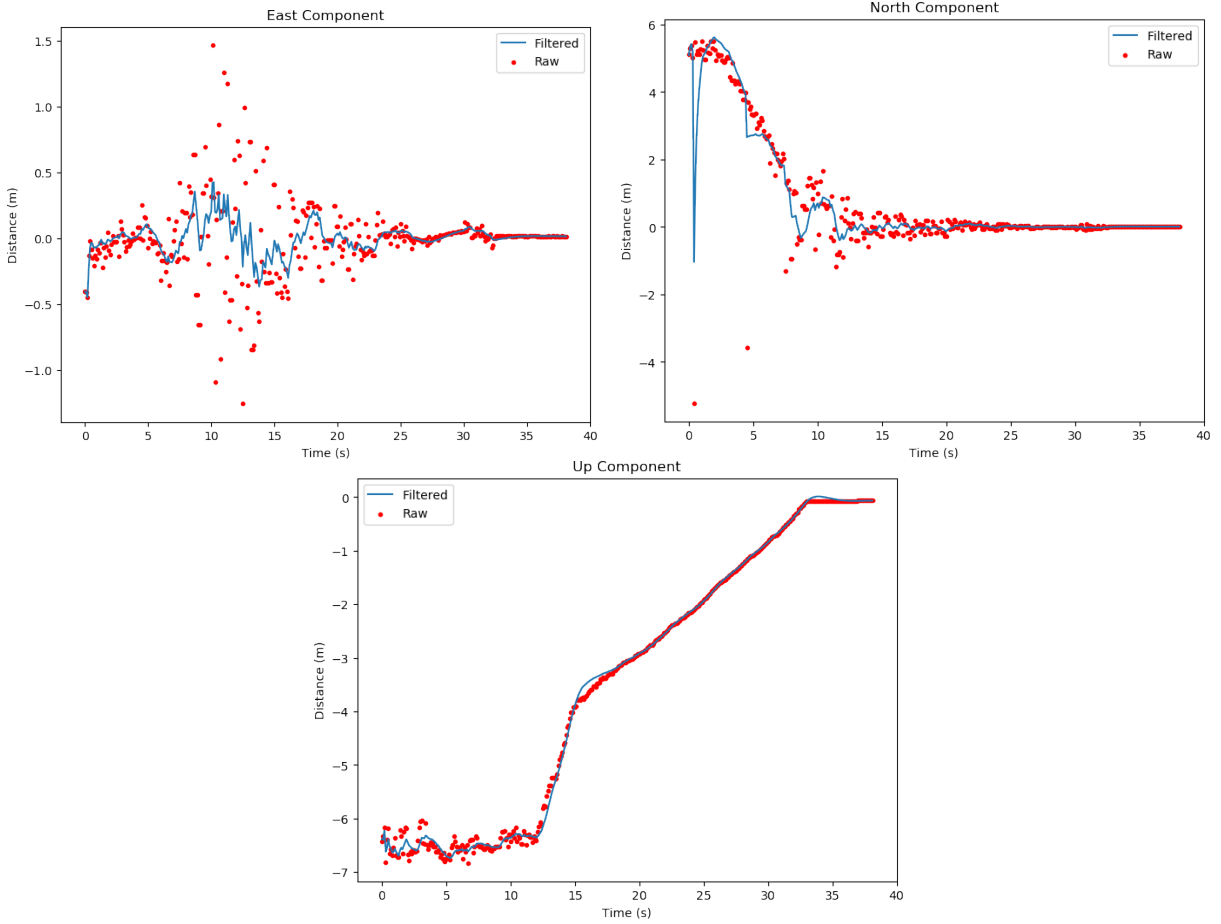


Figure 2.19: Unfiltered and filtered estimates of the landing pad’s position during landing.

such as PX4’s precision land function, a single orientation flip can make the landing fail. This is because the method involves approaching the landing pad horizontally first (facing the landing pad directly), and then descending vertically once the drone is adequately close. The algorithm assumes it has reached or surpassed the landing pad location once it gets a single erroneous pose estimate for the landing pad.

One way around this issue is to simply filter the raw position estimate data with a Kalman filter, as shown in Figure 2.19. The red data points represent the raw data, and the blue, continuous line represents the filtered position estimate that is passed to the PX4 flight software. Since the drone approaches the landing pad head-on, the “north” component of the landing pad’s position is typically the largest. (This is just to say that the landing pad is in front of the drone, not to the side.) Thus, filtering is most important in the case of the north component. If the orientation flips (thereby causing a sign flip in the position), the drone will think that it has already passed the landing pad, and will attempt to land wherever it happens to be when the flip happens. The particularly dangerous data points are therefore the negative outliers in the early stages of the landing. Filtering is useful on the east component to reduce noise. Filtering is not essential on the up component because orientation flipping does not change the perceived height. Variation in the up component is simply considered noise. In spite of the fluctuating raw and filtered values, the position estimate data can be used for precision landing, as demonstrated in Figure 2.20 which shows the horizontal distance from the landing pad versus altitude for multiple such landings. A video of an example landing using the method is available online.<sup>3</sup>

<sup>3</sup>Example landing using PX4’s preland: <https://vimeo.com/625488249>

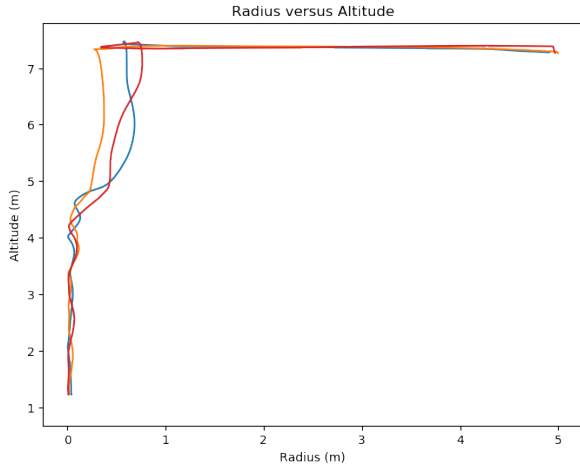


Figure 2.20: Horizontal distance from the landing pad versus altitude for 3 PX4 precision landings using the filtered April Tag 24h10 system. This graph should be read as if the drone is approaching from the right and moving left.

#### 2.3.4 Conclusion

Both the April Tag and WhyCon/WhyCode systems suffer from fundamental issues of orientation ambiguity. April Tag's more intricate structure makes its perception of orientation more robust than that of WhyCon/WhyCode, but it still does not eliminate the ambiguity entirely, and we can see the destructive consequences of this if the orientation is used in other calculations. Still, simple Kalman filtering can mitigate the issue enough that the system can be used for precision landing. Furthermore, the flexible layout of April Tag makes it a better choice for precision landing. The ability to embed concentric markers within each other is critical to maintaining a continuous view of the landing pad from both near and far, and the ability to change the number and layout of data bits allows users to adjust the markers according to their computational constraints.

### 2.4 Experiments with AirSim

#### 2.5 Small Drone

In an effort to avoid some of the logistical limitations induced by the larger drones, e.g. transportation, material costs in the case of crashes, maintenance, overhead from the creation of component covers and mounts, and the use of large batteries, I have adapted a drone design [3] from Thingiverse.com for the purposes of autonomous landing. The base design is a very simple quadcopter platform with a large area for mounting electronics, a flexible motor mount, a symmetric arm design which allows all arms to be interchangeable with one another, and a simple press-fit system for attaching the arms to the body. After modifications, it now includes a pitch-gimbal mount for a Raspberry Pi camera module that is controlled by a micro servo, mounting holes for various components (including the Raspberry Pi, power distribution board, metal legs, and standoffs for an “upper deck”). All modifications were made with OpenSCAD and are available in the drone’s github repository [10]. The drone runs on a 3S (11.1V) lithium polymer power system, with a DJI Snail propulsion system.



Figure 2.21: The IR drone in flight with Joshua (left) operating the drone and Baldur (right) operating the gimbal.

## 2.6 Heavy Lift Drone with Infrared Camera

Drone-based remote sensing is a new and powerful tool in many fields, including geology. To this end, Geologist Christopher Hamilton brought a heavy lift drone to Iceland with the plan of collecting infrared video at active lava sites. The drone is theoretically capable of lifting itself with an extra load of 25 kg. This high weight capacity is necessary to lift multiple large batteries, a large gimbal, and an infrared camera (FLIR). The drone before flight can be seen in Figure 2.22. Along with Baldur, I assembled and tested the drone, making modifications to accomplish the goal of obtaining aerial IR footage of the lava field in Geldingadalur.

The drone uses a WuKong (DJI) industrial flight controller, 6 2-horsepower motors, a 22.2 V, 22000 mAh LiPo battery, and has a diameter of more than a meter. It sits on a gimbal with the mounted IR camera. The gimbal uses a 14.8 V battery to control the orientation of the camera, and receives RC signals from a secondary, dedicated receiver. (One operator controls the drone while the other controls the gimbal.) The camera does not have stringent power requirements, but in this setup the only option for powering it was to provide a 48 V PoE (Power over Ethernet) source. A Raspberry Pi 3 connects to the camera over ethernet and records the streamed video to a file, using a special version of GStreamer developed for the FLIR.

Due to time constraints (about 48 hours from receipt of the gimbal to flying over the lava field), much of the drone has been quickly improvised. Many of these things must be rectified in the near future for further testing. For example, the mounting plate between the gimbal and the drone is completely inadequate (too flexible, not enough points of contact, etc.), and must be replaced with a more solid/purpose-made mounting plate. The 48 V requirement of the camera required an additional 3 4S battery packs wired in series and injected into the ethernet, and this can be replaced with a transformer that can generate 48 V from the same 14 V power source that the gimbal uses. The IR video is not streamed to the operators during flight, so the operators must guess what the camera is seeing, and attempt to obtain good footage.

Still, even with all these disadvantages, the drone flew successfully two times over the lava field at Geldingadalur and obtained aerial IR footage of the lava, as can be seen in Figures 2.21 and 2.23. Additionally, the BBC program documenting the event<sup>4</sup>, and the raw IR footage<sup>5</sup> can be found online.

<sup>4</sup>BBC program documenting the drone flight: <https://www.youtube.com/watch?v=6SIgFPhhRPE&t=1190s>

<sup>5</sup><https://vimeo.com/580302507>



Figure 2.22: The assembled drone before flight.

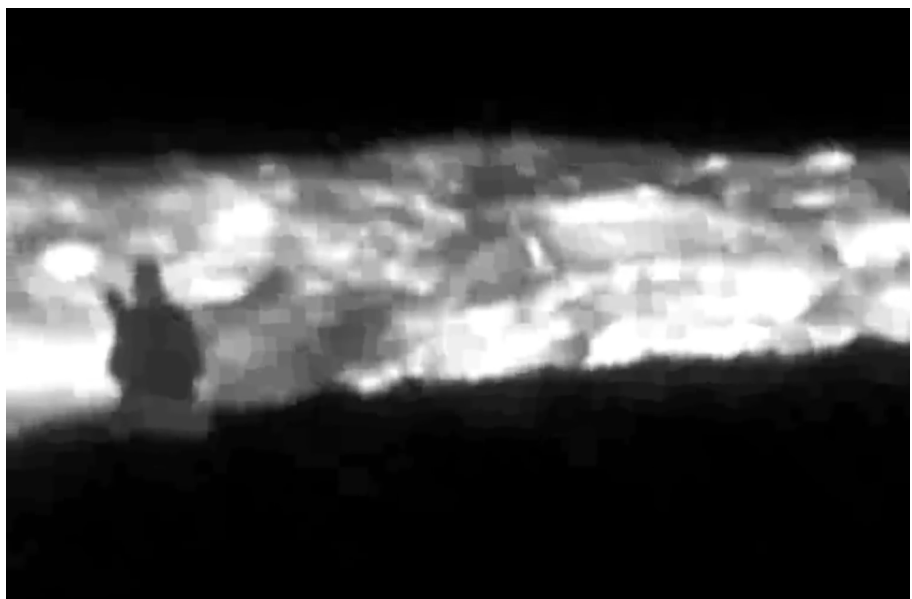


Figure 2.23: An example still picture from the IR footage of the drone.

# Chapter 3

## Research Plan

### 3.1 Data Set Generation

### 3.2 Terrain Classifier Creation

### 3.3 Testing in Simulation

### 3.4 Testing on Physical Hardware

### 3.5 Choice of Flight Software

There are two general stages of testing in the context of drone control algorithms: testing in simulation and testing in the real world. Testing in simulation is an intuitive first step in testing, as it allows to test control algorithms without added logistical, time, or financial cost. It also provides an idealized world, free of complicating factors such as wind, battery life, noisy sensors, etc., isolating the control algorithm as the only testing variable. However, simulation does not prove that a system works in real life. Therefore, after control algorithms have been proven to work in theory (simulation), they must prove themselves again in the real world, with all the implied complexities.

ArduPilot and PX4 are key software packages that can be used for testing in simulation. Previous work in this project and in others have proven worthiness of PX4 and Gazebo in terms of simulated autonomous control. They have complete integration with both simulation environments that are of interest in the upcoming research: Gazebo and AirSim. Both softwares have APIs in Python, C++, and ROS. This research requires position control - and particularly body offset position control. This means that the drone must follow a position setpoint that is given in the coordinate frame that is centered on the drone's body and oriented with the same heading as the drone. The position setpoint is given in terms of ENU (East, North, Up) where East refers to the drone's right, North refers to the drone's front, and Up refers to the drone's top. The setpoint is given in meters, so a position setpoint of  $(E, N, U) = (-2, 1, -1)$  means that the drone should move 2 meters to the right, 1 meter forward, and 1 meter down. In ArduPilot, this type of body offset position setpoint is technically supported, but the firmware translates the position setpoint directly to a GPS coordinate and relies on GPS for navigating to that place. PX4 works also offers an API for generating body offset position setpoints. in some cases the position setpoint must be translated into the NED (North, East, Down) frame, by simply switching the North and East components, and negating the Up component to form the Down component. In PX4, precision land setpoints are only supported in the coordinate frame centered on the drone's home (takeoff) position, and oriented due north, and the coordinate frame is referred to as `LOCAL_NED`. For generating a body offset position setpoint, one therefore

must add the current position and heading to the target position and heading, but otherwise it works in a similar way to the position setpoints. Both ArduPilot and PX4 also offers APIs for controlling a gimbal to aim cameras. In ArduPilot this can be done with an RC override command, where RC input can be programmatically generated and then forwarded to the output channels that control a gimbal. PX4 provides a more sophisticated `vmount` interface that controls the gimbal with possible (user-configurable) consideration of the orientation of the drone.

### 3.6 Risk Analysis

# Bibliography

- [1] Ardupilot.org.
- [2] Edited April Tag Repository. (accessed: 2021.3.25).
- [3] Thingiverse (arks007). Raspberry pi drone (niacam: Txsef 2016-2017). (accessed: 2021.9.24).
- [4] Dronecode. MAVLink Micro Air Vehicle Communication Protocol. (accessed: 2021.5.19).
- [5] Emlid. Navio2. (accessed: 2020.6.5).
- [6] M. Krogius, A. Haggenmiller, and E. Olson. Flexible Layouts for Fiducial Tags. In *2019 IEEE/RSJ International Conference on Intelligent Robots and Systems (IROS)*, pages 1898–1903, 2019.
- [7] Lorenz Meier. Pixhawk. (accessed: 2020.6.5).
- [8] Matias Nitsche and Tomáš Krajník. Original whycon ros github repository. (accessed: 2021.9.30).
- [9] E. Olson. Apriltag: A robust and flexible visual fiducial system. In *2011 IEEE International Conference on Robotics and Automation*, pages 3400–3407, 2011.
- [10] Joshua Springer. Raspberry pi drone. (accessed: 2021.9.27).
- [11] Joshua Springer. Whycon ros github repository. (accessed: 2021.9.30).
- [12] Joshua Springer. Autonomous Landing of a Multicopter Using Computer Vision. Master’s thesis, Reykjavík University, 2020.
- [13] Jiri Ulrich. Whycon ros github repository. (accessed: 2021.9.30).
- [14] John Wang and Edwin Olson. Apriltag 2: Efficient and robust fiducial detection. pages 4193–4198, 10 2016.